JOURNAL OF AIRCRAFT
Vol. 45, No. 6, November–December 2008

Evolutionary Multicriteria Design Optimization of Integrally Stiffened Airframe Structures

Lars U. Hansen,* Sascha M. Häusler,† and Peter Horst‡
Technical University of Brunswick, 38108 Braunschweig, Germany

DOI: 10.2514/1.30884

In industrial practice, innovative structural aircraft design is, on the one hand, driven by several design criteria like static stress, damage tolerance, and stability, and, on the other hand, by new manufacturing methods and materials, which promise beneficial effects on manufacturing costs and weight. Published optimization approaches are mostly based on pure static stress criteria, albeit the important influence of stability and damage tolerance is neglected. This assumption is perilous but significantly simplifies the investigation. The investigation of unconventional designs under consideration of the preceding criteria is challenging because no analytical or handbook solutions are available. This paper introduces an optimization approach based on an *evolution strategy*, which incorporates multiple criteria by using nonlinear finite-element analyses for stability and a set of linear analyses for damage-tolerance evaluation. To demonstrate the approach, one design investigation is presented for the window area of a generic aircraft fuselage. The definition of dimensions and the choice of an ideal topology define the optimization problem. The chosen fuselage structure uses an integral design with an innovative combination of window and circumferential frame and is investigated with regard to three load cases that represent relevant in-flight conditions derived from global finite-element analyses.

Nomenclature

A, B, k, C_f, n_f, K_c	=	Forman coefficients
a	=	crack length
a_m, b_m, α_m	=	shape coefficients of the mass mapping function
a_u, b_u	=	shape coefficients of the deflection mapping function
$a_{\mathrm{SIF}}, b_{\mathrm{SIF}}$	=	shape coefficients of the fatigue-response mapping function
$C_{\mathrm{feas}}, D_{\mathrm{feas}}$	=	coefficients of the failure mapping function, feasible state
$C_{\mathrm{limit}}, D_{\mathrm{limit}}$	=	coefficients of the failure mapping function, limit state
d_i	=	design response i
E	=	Young's modulus
G_{I}	=	energy release rate, mode I
G_{II}	=	energy release rate, mode II
g	=	gravitational acceleration
K	=	stress intensity factor
K_{th}	=	stress intensity factor, threshold value
N	=	load cycle
n	=	load factor
p	=	pressure
R	=	stress ratio
t	=	thickness
u	=	longitudinal displacements at the crack surface
v	=	normal displacements at the crack surface
w_i	=	weight factor i
X_i	=	longitudinal force at the crack tip
Y_i	=	normal force at the crack tip
α_d	=	exponent of the deflection mapping function
α_{SIF}	=	exponent of the fatigue-response mapping function
κ	=	life span
λ	=	offspring per generation
μ	=	population size
ν	=	Poisson's ratio
ρ	=	density

Received 9 March 2007; revision received 29 April 2008; accepted for publication 7 June 2008.

*Research Assistant, Institute of Aircraft Design and Lightweight Structures, Hermann-Blenk-Street 35; L.Hansen@tu-bs.de.

†Research Assistant, Institute of Aircraft Design and Lightweight Structures, Hermann-Blenk-Street 35; S.Haeusler@tu-bs.de.

‡Professor, Institute of Aircraft Design and Lightweight Structures, Hermann-Blenk-Street 35; P.Horst@tu-bs.de.

I. Introduction

TODAY'S aircraft fuselage structures normally exhibit a differential design, which is characterized by the assembly of multiple parts. These so-called built-up structures originate from the philosophy of using sheet metal as a base material from which thin-walled wing or fuselage structures can be manufactured by riveting and bonding.

Efforts to investigate structural alternatives are primarily motivated by potential mass reductions and savings with regard to manufacturing costs and time. Increasing cutting speeds and steadily improving fusion techniques, like laser beam welding and friction stir welding, offer new possibilities to create stiffened structures with integral characteristics not limited to today's rectangular stiffening design. This opens up possibilities to specifically adapt the topology and topography of the structure according to the loads to be expected. A detailed investigation on the applicability of integrally stiffened structures is described in [1]. Although it is stated that the technological risks for such an unvalidated airframe structure are relatively high, the payoff is perceived to be equally high.

An investigation of innovative structural alternatives has to pay special attention to different sizing criteria caused by the changes of the design. This is especially true for the damage-tolerance behavior of integrally stiffened structures, which is at a disadvantage compared with common riveted designs. Consequently, the investigation of design alternatives for conventional built-up fuselage structures requires the consideration of multiple load cases and corresponding sizing criteria.

The described study is based on ideas previously presented (e.g., [2]) to integrate the window into the fuselage frame of a metal fuselage to effectively use the employed material and, consequently, save weight. Alternative integral designs for the window area are,

therefore, investigated by using a detailed parametric finite-element model that is capable of representing a wide range of possible alternative designs with varying layouts and adaptable proportions. For demonstration purposes, the investigation considers three different characteristic load cases using linear and nonlinear analyses, including a fatigue load case at limit load, an ultimate load case at maneuver load, and a residual-strength load case at maximum pressurization. Special attention is devoted to the investigation of damage-tolerance and stability behavior, which is significantly influenced by stiffener dimensions and stiffener topology.

This consideration of stability and damage-tolerance behavior is beyond the scope of many other available optimization approaches for aircraft structures.

An approach by Ledermann et al. [3] is also based on the parametric representation of complete aircraft components, and an optimization example with consideration to stress and stability constraints is given for a wing application. The authors use an evolutionary algorithm to improve the rib positions, but the coarse character of the component model impedes the consideration of further constraints (e.g., fatigue).

Kaletta's thesis [4] presents a more detailed investigation of performance improvements of evolutionary algorithms for optimization of aircraft structures, although without the need for further consideration of fatigue criteria due to the limitation to composite designs.

An interesting survey is presented by [5] with emphasis on the integration of significantly different design responses into the optimization task, including a probabilistic investigation and a cost estimation. The example provided in [5] covers many responses at the expense of the structure's attention to detail, which is a stiffened spar with a simple loading assumption.

A current example of strain-energy-based topology optimization in industrial practice is given by [6], which presents an investigation of the rear fuselage structure of the Airbus A400M transport aircraft. A topology optimization is used to find a solution with minimum compliance for multiple load cases, with the objective of minimizing the structural mass. Additional constraints are not considered in the objective of the first step. A second step is performed manually and translates the new topology into an adequate, conventional design, composed of skin, stringers, and frames. A deterministic sizing optimization is used as a third step to size the structure to meet a variety of different requirements, such as fatigue and stability. Although there is no information on the used fatigue criteria, a closed-form solution for rectangular stiffened structures is used, which limits the applicability of the complete method to rectangular stiffened designs.

Another recent optimization task is published in [7]. The application of topology-optimization algorithms on the ribs of an aircraft wing box of the Airbus A380 is shown. The process presented is again based on an initial topology optimization for minimum compliance, followed by a second step to size the new topology. Here again the disadvantage is that many relevant structural responses, such as nonlinear buckling, crack growth, and stress criteria, are not included in the objective function. They can be included in a second step by changing the dimensions but not the topology.

The topology-optimization approaches of [6,7] optimize topologies for minimum compliance, but not necessarily for a Pareto-optimal design under consideration of additional design constraints and limitations. This shows that the application of multicriteria optimizations, considering all relevant criteria in a single optimization step, is rare for aircraft structures, especially when it comes to real-world problems with an appropriate level of detail. A two-step, multilevel optimization approach has been shown by [8] for unconventional aircraft structures by using an evolutionary algorithm and a deterministic optimization method to find suitable designs under different design constraints.

A method of performing such an optimization within a single optimization step is presented in this context: to demonstrate the performance of such a setup, an exemplary optimization model for the window area of a generic aircraft has been developed, which, by using various parameters to control the structural setup, is able to cover a large variety of different designs. The applied optimization approach is based on an evolutionary algorithm.

The objective of the optimization is defined by different design responses that are combined in a single fitness function by the use of mapping functions. These mapping functions ensure the equal treatment of the different response types and allow for an optimization that considers resulting structural mass, stability, damage-tolerance, and residual-strength responses.

The rest of the paper is structured as follows: in Secs. II and III the optimization approach and the parametric models are presented. In Sec. IV the parametric models of the window area and their optimization by means of an evolution strategy are described. Section V summarizes the results, and Sec. VI draws some conclusions.

II. Optimization Approach

The objective of the optimization task is to find a structure that fulfills design requirements and constraints and offers a minimum mass. The scope of the design space covers different model topologies and topographies.

Consequently, the representation of such structural layouts requires 1) design variables that describe the model topology and topography (e.g., existence of additional stiffeners, location of spline control points) and 2) design variables that influence the model proportions and the force flow in the structure by changing the stiffness distribution (e.g., thicknesses, cross-sectional areas).

In this context, an evolution strategy has been chosen to solve the optimization task due to the special challenge in dealing with a mixture of discrete and continuous design variables and a volatile design space.

Evolution strategies and genetic algorithms belong to the group of evolutionary algorithms that are all based on Darwin's theory of evolution: a group of solutions, each one defined by their genes (genotype) and referred to as *individuals*, is put under selection pressure and either reduced by the weakest or selected for recombination by the fittest. This idea of survival of the fittest is simulated over multiple generations to determine the best solution. The capabilities of this method are explained in detail in [8].

III. Simulation Model

The simulation model presented in this context is based on the finite-element method. These models are generated using the commercial pre- and postprocessor MSC.Patran® by making extensive use of the Patran command language.

To increase the computational efficiency, MSC.Patran is executed in command line mode (batch mode). In this case, model parameters are provided by an input file, and suppressed graphics processing helps to further reduce the required time for model generation.

The finite-element models are solved using the commercial finite-element solver MSC.Nastran® with different solution sequences (SOL 101 for linear and SOL 106 for nonlinear analyses) depending on the optimization task.

The evolution strategy used for this investigation is an in-house tool called *EStruct* that is written in Python and based on methods proposed by [9]. The routine makes use of the object orientated features of Python by handling each offspring as a separate instance of a common class. This basic idea leads to a transparent code that is easy to adapt. The current version features possibilities to restart from an earlier run, to distribute jobs on multiple machines (nodes), and to determine the fitnesses externally (e.g., Ansys®, Nastran®) [8].

IV. Optimization of Integrally Stiffened Fuselage Structures

A. Analysis Model

1. *Geometry*

The investigated models represent the window area of a typical short-range single-aisle fuselage structure of a conventional aircraft.

The model features a fuselage radius of 1975 mm, a frame pitch of 520 mm, and a total length of 6 frame stations (equaling 2600 mm). The lower edge of the model is bounded by the passenger floor of the aircraft, and the upper edge is approximately 1450 mm above the floor. To simplify the geometry, a symmetric arrangement with three stringer sections below and above the windows is chosen, whereas the target area of the upcoming optimization is primarily limited to the window section, represented in Figs 1 and 2 by the regions shaded in light gray. This region can then be attached to the surrounding structure either by welding techniques or conventional riveting. The window area itself is assumed to be manufactured by high-performance cutting, as was shown for a similar design by Airbus [2]. It can be seen from Fig. 3 that the required cutting volume and size of the semifinished part limit the maximum stiffener height that can be realized within the window area.

The geometry of the L-shaped stringers in the surrounding differential part is fixed to a height of 25 mm, a head width of 8 mm, a foot width of 25 mm, and a uniform thickness of 2 mm.

As a reference for following investigations, a structural design with frames located between the windows is defined. This configuration resembles a common airframe design and is shown in Fig. 1. Because of its similarity with conventional differential structures, this design is used for evaluation of all alternative designs during the following optimization task. The basic alternative design is then created by moving the window into the frame thus creating a new innovative design, JWF design (joint window frame design) (cf. [2]).

This topology forms the basis for all further investigations and will be the subject of optimization by including additional design variants, which will be presented in more detail in the following sections. The design is characterized by merging the function of frame and window and is depicted in Fig. 1 with an arrangement of various stiffeners around the window. These stiffeners form the basic topology and are subjected to the optimization task.

In all the investigations the frame is attached directly to the skin, and all frame dimensions remain constant with a height of 110 mm, a thickness of 2.5 mm, and a frame head width of 24 mm.

Because of the preceding idea of combining frame and window tasks, the window frame height is also subjected to the optimization. The lower limit is defined by the window frame height of the differential structure, which is 30 mm. The upper limit is restricted to 60 mm to account for the previously mentioned manufacturing restrictions (cf. Fig. 3) and requirements from the cabin design.

The window size is modeled to be variable, but it is fixed during the following investigations. The size of the window is defined according to typical window dimensions with a size of 193×150 mm and a corner radius of 135 mm. The dimensions of the window rest remain constant with a width of 22 mm and a thickness of 6 mm. The window frame thickness is uniformly set to 4.5 mm.

The skin thickness for the present example is fixed to 2 mm in all skin areas of the window section (integral part). This should be the subject of future investigations due to its additional weight-saving potential. However, no variation of the skin thickness is performed for the following optimization.

The structural mass of the complete reference structure, as shown in Fig. 1, is determined using volume information from the finite-element model and defined material density, and it is approximately 35.5 kg for a window frame height of 30 mm.

2. *Load Cases*

The following three load cases are considered for the presented optimization task: a fatigue load case, with recurring loads at limit load level and cabin pressure; an ultimate load case with maximum fuselage bending including a safety factor of 1.5; and a residual-strength load case at maximum pressurization of $2\Delta p$ (cf. Table 1).

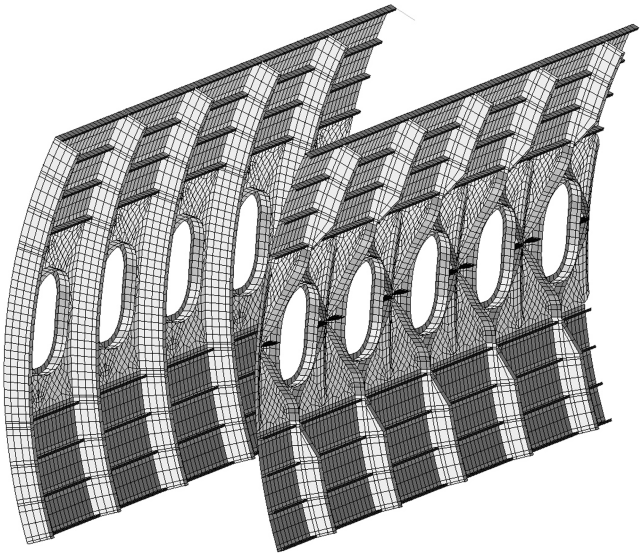

Fig. 1 Conventional fuselage window panel design with reference structure (top) and integral JWF design (bottom).

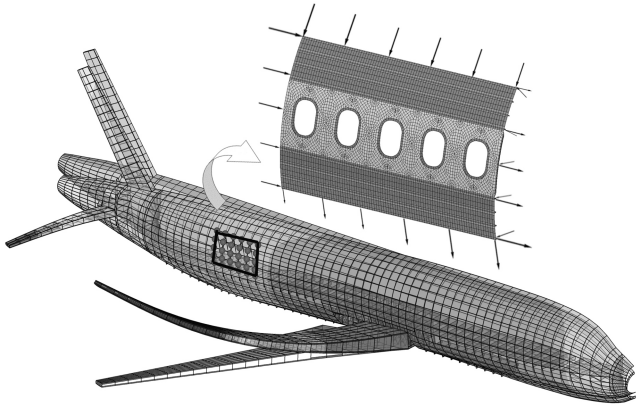

Fig. 2 View of the loads source, displacement loads from global FEM of PrADO/SAM models.

Loading conditions for the fuselage section under investigation are applied via nodal deformations (displacements and rotations) along the edges of the FE (finite element) model and element surface loads for the cases in which pressurization is to be modeled.

Except for the residual-strength load case with $2\Delta p$ pressurization, the applied deformations are extracted from FE simulations using a global discretization of the aircraft, created with the integrated preliminary aircraft design software PrADO (Preliminary Aircraft Design and Optimization) [10], which is a multidisciplinary design software with different modules for each major design discipline. Based on a parametric description of all independent design variables of the aircraft, multidisciplinary analyses are performed in an iterative procedure until a consistent and convergent design of all dependent design variables is achieved (e.g., convergence on required fuel mass, structural mass, required thrust).

Table 1 Load cases

Load case	Loads origin	Load/flight condition	Cabin pressure	Load factor	Scaled by factor of safety
1	PrADO/SAM global FEM	Maneuver	None	$n \approx 2.5$ g	$j = 1.5$
2	PrADO/SAM global FEM	cruise + 10%	$1\Delta p = 615$ mbar	$n \approx 1.0$ g	$j = 1.0$
3	$2\Delta p$ only	Residual strength	$2\Delta p = 1230$ mbar	n/a	

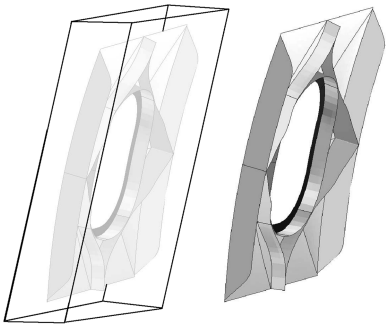

Fig. 3 Semifinished section before (left) and after high-performance cutting (right). Maximum stiffener height is limited by dimensions of semifinished parts.

One of these modules handles the assessment of the elastic behavior of the aircraft, the sizing of the structure, and the prediction of the primary and secondary masses. The corresponding method is based on a finite-element model generated by the module PrADO/SAM (PrADO/Structural Analysis Module). This model is loaded by inertia loads of the payload and the aircraft and by aerodynamic loads calculated with an aerodynamic panel code (see [11] for further details). Because of the fully automated, parametric setup, the program is able to cover a large variety of different aircraft designs (e.g., [12–15]). As a spin-off, a global aircraft finite-element half-model with consistent and physically profound loads is available for further investigation (cf. [11]). The resulting nodal deformations are extracted from this model and are then applied to the corresponding nodes in the detailed model of the investigated alternative structure (as depicted in Fig. 2). Beam elements, with artificially high stiffness, are used as a kind of load frame along the model edges to reduce singularity effects induced by the discrete load introduction.

3. *Fatigue Model*

As mentioned in the preceding section, the damage-tolerance behavior is one of the main issues for the structural sizing of integral designs. Because the structural parts are quite different compared with the ordinary design, more elaborate investigations are needed here. To identify representative cases, the assumption is made that fatigue behavior is assessed by crack-growth calculations for one specific damage scenario. In this context, an extending crack, which initiated at the window and has resulted in a breakage of the window frame, is considered to be the critical damage scenario and is, therefore, adopted for the investigations of the fatigue behavior. The described crack scenario is depicted for one exemplary crack length in Fig. 4. Load case 2, as defined in Table 1, is used for these fatigue investigations, because it represents the typical loading conditions during normal service.

The crack growth rate is calculated by Forman's equation [16]:

$$\begin{aligned}
&\Delta K \le \Delta K_{\text{th}}\text{:}\ \frac{\mathrm{d}a}{\mathrm{d}N} = 0\\
&\Delta K > \Delta K_{\text{th}}\text{:}\ \frac{\mathrm{d}a}{\mathrm{d}N} = \frac{C_f \cdot (\Delta K)^{n_f}}{(1-R)\cdot K_c - \Delta K}\\
&\Delta K \ge (1-R)\cdot K_c\text{:}\ \frac{\mathrm{d}a}{\mathrm{d}N} = \infty
\end{aligned} \tag{1}$$

The required load cycles for a defined crack propagation can be determined by integration of $\mathrm{d}a/\mathrm{d}N$,

$$N(a) = \int_{a_1}^{a_2} \frac{(1-R)\cdot K_c - \Delta K}{C_f \cdot (\Delta K)^{n_f}}\,\mathrm{d}a \tag{2}$$

Based on stress intensity factor solutions for five given crack lengths, a quadratic expression, relating stress intensity factor K to crack length a, can be determined using polynomial spline fitting. The stress intensity factors are determined by means of a technique that is based on the crack closure method.

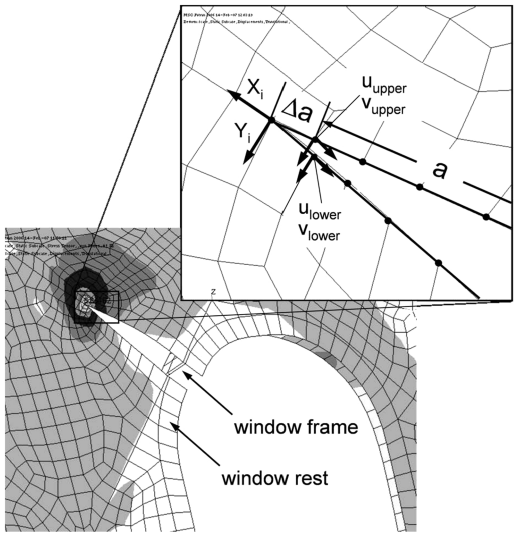

Fig. 4 Crack tip model for application of the VCCT; the upper surface forces at the crack tip are omitted for clarity.

The crack closure method assumes that the work required to close the crack is proportional to the energy released when the crack is extended. The forces and the displacements of a pair of nodes close to the crack tip are used to calculate the work required to reestablish the original, uncracked condition. These forces are consequently identical to the forces acting on the upper and lower surface of the closed crack. Two states are therefore needed to determine the energy release rate G: one analysis to calculate the forces for the closed crack and another analysis to calculate the forces and opening displacements for the open crack.

A modified technique, called virtual crack closure technique (VCCT), introduces the additional assumption that a crack extension of small Δa does not change the state at the crack tip significantly, which consequently allows for a one-step evaluation by using the results of a single linear finite-element analysis. The necessary energy release rate G, needed for a virtual extension of the crack, is assumed to create the same crack opening displacement as for the unextended crack [17].

Figure 4 illustrates the required parameters needed for employment of the VCCT for one exemplary crack length of the investigated damage scenario.

Using the VCCT for four-noded 2-D elements, the energy release rate is then defined by the following relations (cf. [17]):

$$G_{\text{I}} = -Y_i \cdot \frac{(v_{\text{lower}} - v_{\text{upper}})}{2\cdot \Delta a \cdot t} \tag{3}$$

$$G_{\text{II}} = -X_i \cdot \frac{(u_{\text{lower}} - u_{\text{upper}})}{2\cdot \Delta a \cdot t} \tag{4}$$

Assuming linear elastic fracture mechanics and a plane stress state, the energy release rates G_{I} and G_{II} can be directly related to the stress intensity factors K_{I} and K_{II}

$$K_{\text{I}} = \sqrt{G_{\text{I}} \cdot E} \tag{5}$$

$$K_{\text{II}} = \sqrt{G_{\text{II}} \cdot E} \tag{6}$$

For simplification, only the governing mode I stress intensity factor K_{I} will be considered for succeeding crack growth calculations. Nevertheless, it should be mentioned that significant stress intensity factors for mode II and mode III were observed for certain crack lengths during the investigation, which suggest that the extending crack might be subjected to crack turning or deflection. However, analysis of these effects requires more detailed examinations and is

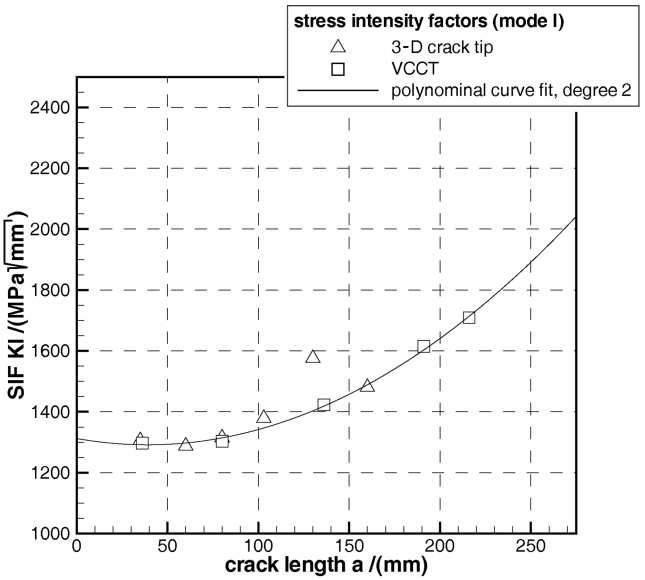

Fig. 5 Stress intensity factors from 3-D crack tip analysis, VCCT, and curve fit.

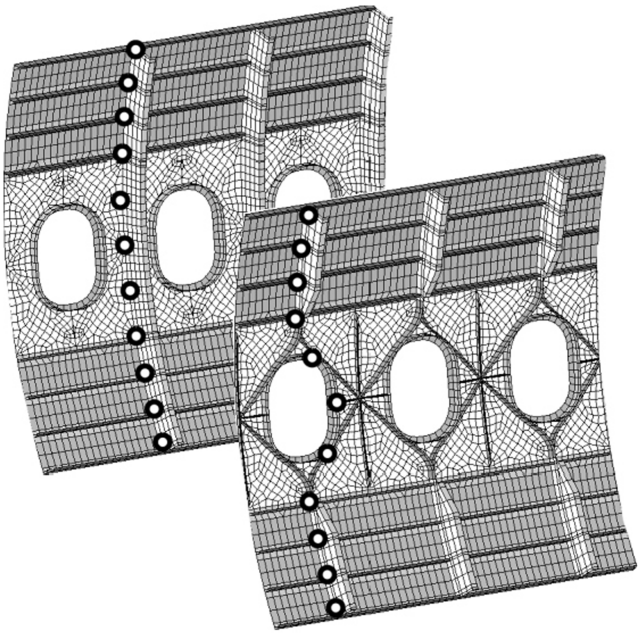

Fig. 6 Displacement results path for nonlinear deformation investigation: differential (top) and integral (bottom) design.

beyond the scope of the present work, which is focused on the structural optimization task.

The required number of load cycles, to grow the crack from an initial to a maximum crack length, is taken as a measure to evaluate the fatigue behavior. The initial (detectable) corner crack length is set to 20 mm and the maximum crack length is defined by the position where the crack reaches the first stiffener of the surrounding regular structure ($a_{\max} = 250$ mm).

The stress intensity factor results of the VCCT are verified with a 3-D finite-element model, based on a detailed discretization of the crack tip, using degenerated 20-node quarter-point elements (Barsoum-type elements).

Figure 5 compares the resulting mode I stress intensity factors, which are determined using the 3-D crack tip model and the VCCT. The comparison shows good accordance between both methods, which confirms the application of the VCCT for the presented paper. The polynomial fit that approximates the VCCT results and is used for succeeding crack growth calculations is also depicted.

4. *Nonlinear Stability Model*

Buckling stability is the second important criterion to be considered in the following optimization. Again the fact that the skin areas do not exhibit a conventional stiffening design requires a more detailed assessment of the stability response. Because the generic stiffening character of nonrectangular fields yields no typical buckling limits, another approach is proposed to enable a judgment on the stability behavior under maximum bending load (cf. ultimate load case 1 in Table 1). As a measure of the deformation level, radial displacements along a vertical analysis path are determined, which allow for an evaluation of the global buckling behavior of the structure. This seems to be the more appropriate stability criterion in this context because local buckling is obviously not such a fixed criterion nowadays.

The investigated deformation path for the reference structure is defined by nodes at the frame–skin intersection in a vertical direction. Because of the incorporation of the window into the frame, a slightly different path has to be chosen for the alternative designs (cf. Fig. 6) with adapted node positions in the window belt region caused by the new frame topology.

As a result of applying nodal displacements from a global FE simulation, the investigated structure exhibits significant rigid body motion in addition to its deformation, and this complicates the determination of the relevant radial displacements along the analysis path. This problem is solved by performing two consecutive analyses of the considered structure: one nonlinear simulation of the real, unaltered structure that undergoes rigid body motion and global radial deformation and one linear simulation of the same structure with artificially high stiffness properties in all skin regions that undergoes the same rigid body motion but exhibits no other deformations. Using the results from both simulations (displacements in x, y, z direction) along the analysis path, it is possible to cancel out the rigid body motion, which yields the pure radial deformation along the vertical path.

This procedure is applied to every structure that is investigated during the optimization process, including the built-up reference. The following two fitness indicators are defined for evaluation of the stability behavior as one part of the global design objective:

1) The maximum-displacement criterion is the comparison between maximum displacements of the alternative and reference structures.

2) The similarity criterion is the least-squares sum of the differences between reference and alternative structure for each position along the analysis path.

5. *Material Properties*

The material properties are based on a typical aircraft aluminum of type 7475T7351, with elastic properties including a Young's modulus of $E = 71,700$ MPa, Poisson's ratio of $v = 0.3$, and density of $\rho = 2.8 \cdot 10^{-6}\text{kg/m}^3$.

Changes in the crack growth parameters due to the effect of specimen thickness on the resulting crack resistance/fracture toughness (see [18]) are neglected. The parameters for the Forman equation, including $A = 87$, $B = 1$, $k = 1$, $C_f = 3.39 \cdot 10^{-7}$, $n_f = 2.32$, and $K_c = 2473\text{MPa}\sqrt{mm}$, were taken from [16].

B. Design Variables

The design variables of the model can be subdivided into one group of parameters influencing the model topology and one group of sizing variables that affect the model dimensions. The major design variables are depicted in Fig. 7. An important feature of the parametric model is to allow for all possible combinations of stiffener existence or absence.

Smoothly running stiffener topologies are defined that can only be achieved by welding or milling and that provide a soft load transfer between skin and stiffeners. The exact shape is controlled by different spline functions using control points to define the local height of the stiffener. This discretization also enables a continuous modification of the stiffener shape rather than being limited to a

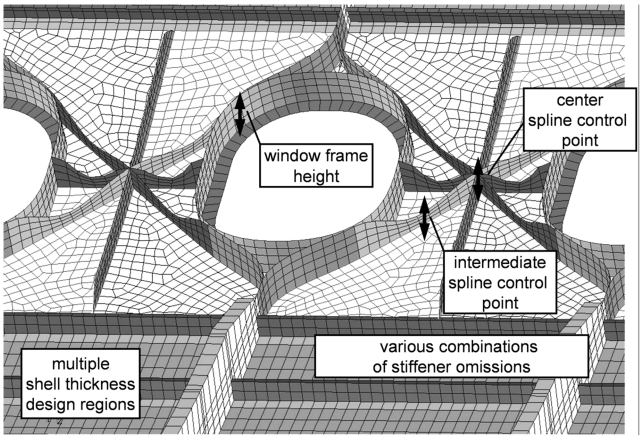

Fig. 7 Design variables of the optimization model.

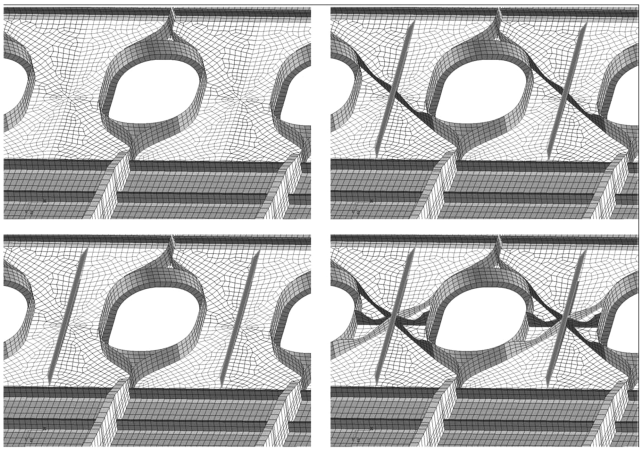

Fig. 8 Finite-element models of different stiffener topologies between the windows.

number of fixed heights. The thicknesses and the cross-sectional area are used as additional design variables.

An overview of all design variables and their side constraints is given in Table 2. To give an impression of different stiffener topologies, a few possible combinations are shown in Fig. 8.

C. Design Objective and Fitness

The investigation of different model parameters requires a common fitness indicator to rate the concepts. The following investigation uses the structural mass, resulting from the structure's density and volume, the deflection, the bearable load cycles, and the residual strength to rate the performance.

In the optimization setup, all these values are included in a single fitness function by the use of mapping relations (as shown by [19,20]). This leads to an optimization objective in which the fitness is not only defined by the mass but also by the conformance with design constraints.

A very common method for multi-objective optimization is the weighted-sum approach. Minimizing the objective function $f(X)$ is sufficient for Pareto optimality [21]. The weight function is defined as

$$f(X) = \sum_{i=1}^{n} w_i \cdot d_i \tag{7}$$

with w_i being weight factors (positive, here set to 1) and d_i representing the results of i different design responses.

These responses have been translated by mapping functions in such a manner that a low value (e.g., zero) represents the desired condition. Undesired conditions (e.g., stress violations, excessive masses, large displacements) create responses of $d_i > 0$. The mapping functions are normally defined in the range of $0 \leq d_i \leq 1$ to avoid unequal treatment of the different responses.

Mapping functions, presented in [19], have been adapted to the given problem as follows:

1. *Mass Response Mapping Function*

The mass mapping function relates the structural mass to a mass response value. A function has been chosen that penalizes masses above a maximum level exponentially:

$$d_1(\text{mass}) = (a_m \cdot \text{mass} + b_m)^{\alpha_m} \tag{8}$$

The coefficients a_m and b_m are calculated before the optimization by definition of lower and upper limits so that

$$d_1(\text{mass} = m_{\text{lower}}) = 0.1 \tag{9}$$

and

$$d_1(\text{mass} = m_{\text{upper}}) = 1.0 \tag{10}$$

The lower limit is defined by a mass saving of approximately 10% with respect to the reference structure (32.265 kg). The upper limit is set to 40 kg and the exponent α_m to $\alpha_m = 5$ (cf. [19]).

2. *Deflection Response Mapping Function*

The deflection of the structure is also linked by an exponential mapping function to the structural response:

$$d_2(\text{deflection}) = (a_u \cdot \text{deflection} + b_u)^{\alpha_d} \tag{11}$$

To determine the coefficients a_u and b_u, multiple preanalyses of the reference and of the alternative structure are performed where the structural alternatives show more deflection than the differential reference structure due to the reduced bending stiffness in the frame–window area and the different analysis path (cf. Fig. 9). To derive a suitable indicator for the global buckling behavior, the maximum displacement (cf. maximum-displacement criterion in Sec. IV.A.4) is therefore allowed to be 85% higher than the reference structure to achieve a fitness of 0.1.

The deformation shape, rated by the least-squares sum of differences between reference and alternative structure (cf. similarity criterion in Sec. IV.A.4), is treated by a similar fitness function but with different coefficients. As mentioned, a larger deformation of the integral design seems to be reasonable and tolerable. The exponent α_d was set to $\alpha_d = 5$.

3. *Fatigue-Response Mapping Function*

The fatigue quality of the structure is characterized by the number of bearable load cycles available until the crack is extended to a total

Table 2 Design variables

No.	Design variable	Type	Minimum	Maximum
1	Intermediate stiffener height	Spline control point	10 mm	60 mm
2	Center stiffener height	Spline control point	10 mm	60 mm
3	Window frame height	Constant height	30 mm	60 mm
4	Vertical stiffener	Existence/abscence	Yes	No
5	Cross stiffener	Existence/abscence	Yes	No
6	Horizontal stiffener	Existence/abscence	Yes	No

length of $a_{\max} = 250$ mm, corresponding to the location of the nearest stiffener. The applied mapping function is again an exponential relation defined by

$$d_3(N) = (a_{\text{SIF}} \cdot N + b_{\text{SIF}})^{\alpha_{\text{SIF}}} \tag{12}$$

The factors a_{SIF} and b_{SIF} are used for calibration to the desired optimization goal (see the description in the previous section). The exponent α_{SIF} was set to $\alpha_{\text{SIF}} = 5$.

As already mentioned, cracks are more severe in integral structures than in differential structures. To account for this, more than twice as many load cycles as for the reference (differential) structure are set as the optimization goal. With an initial crack length of 20 mm, already detectable by general visual inspection, a total number of $N \approx 8500$ load cycles[§] is bearable by the reference structure until maximum crack extension is achieved. The factors a_{SIF} and b_{SIF} are chosen to relate the optimization goal to the desired fitness values of

$$d_3(N = 17,000 \text{ load cycles}) = 0.1 \tag{13}$$

and

$$d_3(N = 11,000 \text{ load cycles}) = 1.0 \tag{14}$$

emphasizing the desire to significantly improve the fatigue behavior of the integral alternative.

4. *Failure/Residual-Strength-Response Mapping Function*

The residual strength of the structure is evaluated by the stress intensity factor for load case 3 and a significant damage of 90% maximum crack length ($a_{\text{res}} = 90\% a_{\max}$). A step function with smooth transition between best ($d_4 = 0.01$) and worst ($d_4 = 1.0$) fitness level is used. For all cases in which $K(a_{\text{res}}) \leq K_c$ (cf. Sec. IV.A.3 about the fatigue model), the lowest fitness of 0.01 is contributed to the overall fitness function. For values of $K(a_{\text{res}}) > K_c$, fitness values between 0.01 and 1.0 are assigned.

The following relations are used:

$$d_4(k) = \frac{1}{1 + e^{-\lambda \cdot (\frac{K}{K_c} - \Delta)}} \tag{15}$$

with

$$\lambda = \frac{1}{C_{\text{feas}}} \left(\ell n \left(\frac{1}{D_{\text{limit}}} - 1 \right) - \ell n \left(\frac{1}{D_{\text{feas}}} - 1 \right) \right) \tag{16}$$

and

$$\Delta = \frac{1}{\lambda} \ell n \left(\frac{1}{D_{\text{limit}}} - 1 \right) + 1 \tag{17}$$

The shape of the step function is influenced by the constants D_{feas}, C_{feas}, C_{limit}, and D_{limit} that are set to $C_{\text{feas}} = 0.1$, $D_{\text{feas}} = 0.5$, $C_{\text{limit}} = 1.0$, and $D_{\text{limit}} = 0.01$ (cf. [19]).

The residual strength is defined by the failure at a stress intensity of K_c. A value of $K \leq K_c$ results in a fitness of 0.01. Stress intensity factors (SIF), being 5% higher than K_C, already correspond to a fitness of 0.99.

V. Results

A. Reference Structure Versus Alternative Structures

Before the automated optimization, different combinations of design variables were investigated. As described in Sec. IV.C the behavior of the differential design was taken as a reference to calibrate the mapping relations and, thereby, the optimization objective.

Significant differences were observed for the crack growth behavior between the differential and the alternative designs. Although the SIF solutions for the differential reference featured decreasing SIF indicating crack retardation, the JWF design showed an opposite effect with increasing SIF approaching the maximum crack length. This behavior is shown in Fig. 10 for two exemplary configurations.

For the residual-strength load case the SIF were also much lower for the reference structure.

In terms of stability, the differential structure deformed less than the integral structure. In particular the window height, here chosen to be less than 60 mm, significantly reduced the bending stiffness of the frame (normal height 110 mm).

B. Optimization

The evolutionary μ, κ, λ strategy EStruct [8] was used with the settings $\mu = 15$ (population size), $\kappa = 5$ (life span), and $\lambda = 80$ (offspring per generation). The optimization was stopped after 18 generations; in total $18 \cdot 80 \approx 1400$ individuals were modeled and analyzed during the optimization. The model generation and fitness evaluation required ≈15 min for one individual (7 linear static and 1 nonlinear analysis) on an AMD Opteron64, (2.2 GHz, 2 GB RAM) Linux system. In the case of a parallel evaluation on 5 CPUs, 4 h per generation were required (in total 300 CPU h).

Because of the total number of over 1400 individuals, not all of the results can be presented in detail.

The convergence of the optimization approach is shown in Fig. 11 with the development of the fitness over generations. The fitness of the best, the worst, and the average of the population is depicted for each generation. The best individual's fitness improved and the worst individual's fitness remained almost unchanged over the generations. This indicates that the strategy variables, influencing

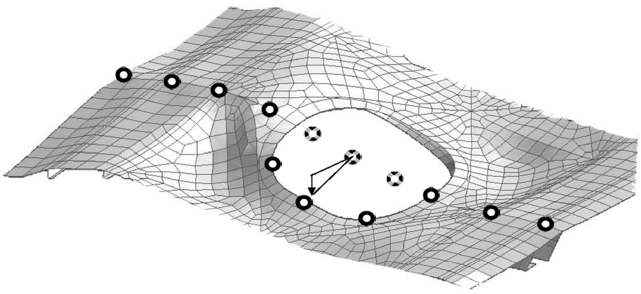

Fig. 9 Increase in measured deformation due to the curved displacement results path through the panel's buckling pattern.

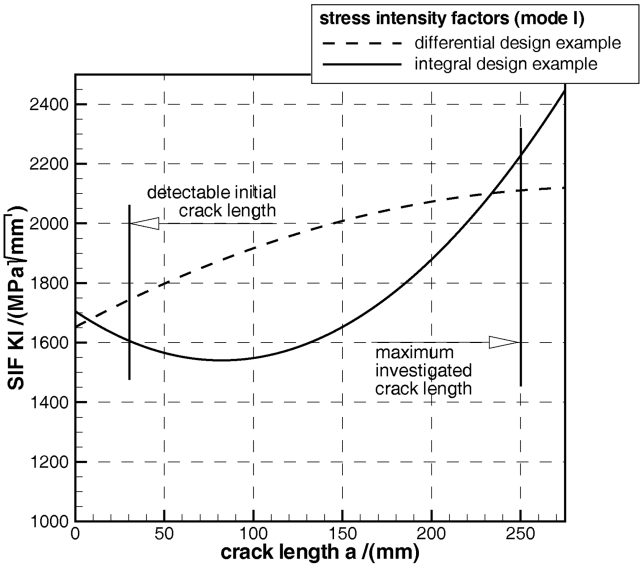

Fig. 10 Integral vs differential structures showing stress intensity factors for the fatigue load case.

[§]All given cycle numbers are without consideration of safety factors.

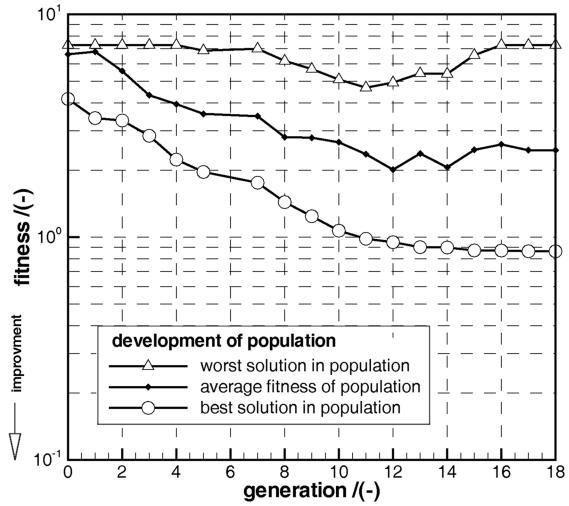

Fig. 11 Development of all contributors to the average fitness of the population.

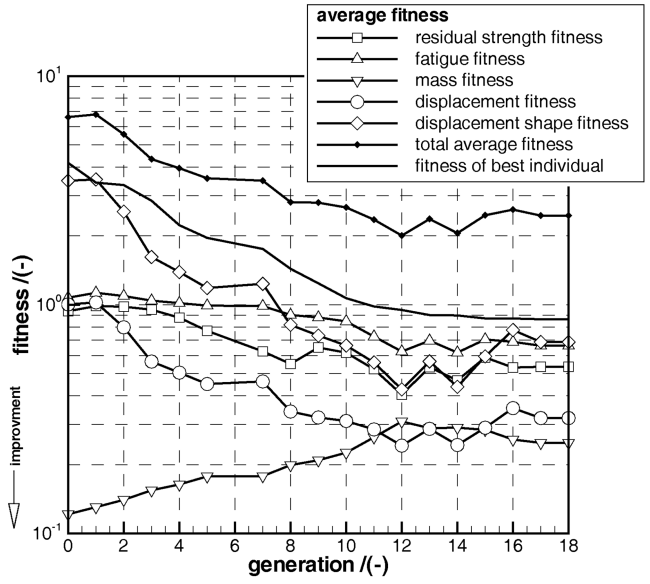

Fig. 12 Average of all fitness addends of each generation.

the mutation strength, did not decrease to zero and that the design variables were still subjected to variations. The final result, after an evolution over 18 generations, hence, has not converged and might still improve. Nevertheless, the significant design changes already prove the applicability of the optimization setup and considerable improvements are unlikely.

To provide an insight into the design improvements, the average fitness (arithmetic average of each generation) is depicted in Fig. 12. Different curves show the changes in the average of the different fitness addends: the average fitness of the fatigue response, the residual strength, the displacement amplitude, and the displacement shape decrease during evolution over 18 generations. Only the average mass of the population increases. For comparison, the fitness development of the best individual is depicted as well.

The overall best JWF design is shown in Fig. 13 and features 1) residual strength with an SIF 4% below K_c, 2) fatigue with twice as many bearable load cycles as the reference structure (integral structure: 16,500 cycles vs differential reference structure: 8490 cycles), 3) a deflection (in the window frame) more than twice as high as the reference, and 4) a mass of 35.76 kg that is 0.7% higher than the reference structure (35.49 kg).

The optimization goal is reached by the residual strength and the fatigue performance. The mass remains constant relative to the

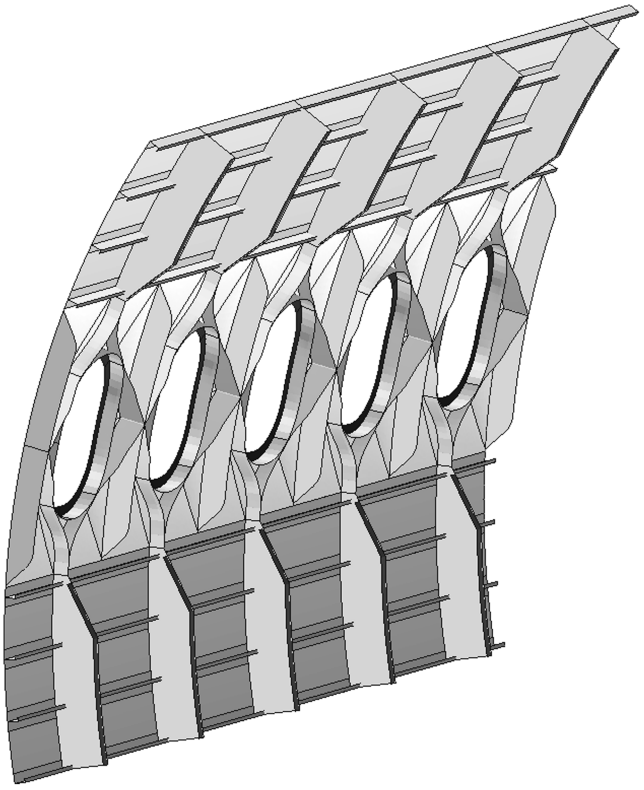

Fig. 13 Optimum JWF design after optimization.

reference, and the deflection is larger due to both the weaker window area and the different analysis path (cf. Fig. 9) being larger. A modified analysis path, or an interpolation between the displacement of both sides of the window frame, might be helpful to put the global buckling behavior into perspective.

The best solution in the present study results in maximum heights of the stiffening members between the windows (spline control points 1 and 2 set to their maximum values). However, a maximum window frame height is not necessary for the best design. The changes of the window height during the optimization are plotted in Fig. 14. The scatter plot shows the 15 best individuals of each generation. The vertical axis denotes the fitness. The horizontal axes are used to plot the development over the generations and the

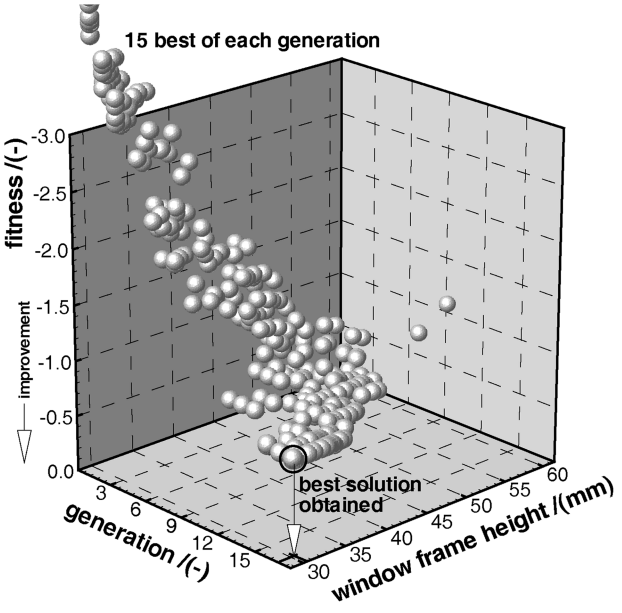

Fig. 14 Window frame height variations during optimization.

changes in the window frame height. The fact that the fitness varies in some cases without changes in the window frame height arises from additional changes in other design variables, which are not shown in the diagram.

In particular, the window frame heights of around 40 mm attract the optimizer due to their contributions to the frame stiffness and their low masses (compared with solutions with much higher frames). Despite the possibility of decreasing the deformation by increasing the window frame height, combinations of design variables leading to small window frame heights produce the best results. Nevertheless, a change in the treatment of the different criteria can produce other Pareto-optimal solutions.

VI. Conclusions

Evaluation of structural alternatives requires the investigation of multiple sensitivities. To rate design alternatives, a method is necessary that is able to optimize parameters and topologies while taking relevant design constraints and requirements into account.

This task can be fulfilled by an evolution strategy that searches for suitable combinations by selection and reproduction of the best combinations found in previous generations. All combinations of parameters, which lead to identical fitness values though composed of different contributors, create Pareto-optimal solutions to the problem.

The main objective of the investigations has been the profound analysis of different structural details and behaviors during an early development stage of airframe structures using an advanced, but computationally expensive, optimization technique. This procedure has been presented in detail without aiming for a final answer to challenges for future lightweight aircraft designs, which is beyond the scope of this work and would require further definition of requirements, loads, and design objectives.

Nevertheless, a method has been introduced that can easily be extended to handle these demands. Furthermore, a structural idea has been created that shows potential to improve today's design principles. These results already prove that the implementation of fatigue and residual-strength criteria allows for an investigation and comparison of different structural designs, even if handbook solutions for the specific problems are not at hand. The proposed idea, an integral design, is based on the use of advanced manufacturing techniques and offers the chance to further industrialize the production of metallic fuselage structures, increasing manufacturing speed and efficiency and, hence, decreasing costs.

The herein presented innovative and unconventional structural idea, called joint window frame design, is a solution that uses the integral manufacturing capabilities by joining the window frame and the frame. The performance of this alternative, integral design is strongly related to the combination of design parameters defining the distribution of stiffeners and their dimensions. A competitive design can only be found by consideration of multiple load cases and design criteria. The solution features more space between the frames, which is beneficial for systems installation and cabin design. However, a disadvantage is the need for larger window frames to contribute sufficiently to the bending stiffness of the circumferential frame. As a consequence, the window frames are likely to be higher than today's design, fortunately simplifying the structural challenge arising from the passengers' desire for larger windows.

The disadvantageous fatigue behavior of the integral design is improved significantly during the optimization, actually exceeding the performance of the reference structure. By adjusting the fitness mapping functions, further and extensive investigation of various load cases and criteria seems feasible to improve the proposed design even further.

References

[1] Munroe, J., Wilkins, K., and Gruber, M., "Integral Airframe Structures (IAS)—Validated Feasibility Study of Integrally Stiffened Metallic Fuselage Panels for Reducing Manufacturing Costs," NASA CR-2000-209337, 2000.

[2] Pacchione, M., and Telgkamp, J., "Challenges of the Metallic Fuselage," *Proceedings of the 25th International Congress on Aeronautical Sciences*, International Council of the Aeronautical Sciences, Hamburg, 2006, pp. 1–12.

[3] Ledermann, C., Ermanni, P., and Kelm, R., "Dynamic CAD Objects for Structural Optimization in Preliminary Aircraft Design," *Aerospace Science and Technology*, Vol. 10, No. 7, 2006, pp. 601–610. doi:10.1016/j.ast.2006.07.001

[4] Kaletta, P., "Ein Beitrag zur Effizienzsteigerung Evolutionärer Algorithmen zur optimalen Auslegung von Faserverbundstrukturen im Flugzeugbau," Ph.D. Dissertation, Technical Univ. of Dresden, Dresden, Germany, 2006.

[5] Xie, Q., and Rais-Rohani, M., "Probabilistic Design Optimization of Aircraft Structure with Reliability, Manufacturability, and Cost Constraints," *44th AIAA/ASME/ASCE/AHS Structures, Structural Dynamics, and Materials Conference*, AIAA, Reston, VA, April 2003, pp. 1–18.

[6] Schuhmacher, G., Stettner, M., Zotemantel, R., O'Leary, O., and Wagner, M., "Optimization Assisted Structural Design of a New Military Transport Aircraft," *10th AIAA/ISSMO Multidisciplinary Analysis and Optimization Conference*, AIAA, Reston, VA, 2004, pp. 1–9.

[7] Krog, L., Tucker, A., Kemp, M., and Boyd, R., "Topology Optimisation of Aircraft Wing Box Ribs," *10th AIAA/ISSMO Multidisciplinary Analysis and Optimization Conference*, AIAA, Reston, VA, 2004, pp. 1–11.

[8] Hansen, L., and Horst, P., "Multilevel Optimization in Aircraft Structural Design Evaluation," *Computers and Structures*, Vol. 86, Nos. 1–2, 2008, pp. 104–118. doi:10.1016/j.compstruc.2007.05.021

[9] Schwefel, H.-P., *Evolution and Optimum Seeking*, Wiley-Interscience, New York, 1995.

[10] Heinze, W., "Ein Beitrag zur Quantitativen Analyse der Technischen und Wirtschaftlichen Auslegungsgrenzen Verschiedener Flugzeugkonzepte für den Transport Grosser Nutzlasten," Ph.D. Dissertation, Technical Univ. of Brunswick, Braunschweig, Germany, 1994.

[11] Österheld, C., "Physikalisch Begründete Analyseverfahren im Integrierten Multidisziplinären Flugzeugvorentwurf," Ph.D.-Dissertation, Technical Univ. of Brunswick, Braunschweig, Germany, 2003.

[12] Hansen, L., Heinze, W., and Horst, P., "Representation of Structural Solutions in Blended Wing Body Preliminary Design," *Proceedings of the 25th International Congress on Aeronautical Sciences*, International Council of the Aeronautical Sciences, Hamburg, 2006, pp. 1–13.

[13] Österheld, C., Heinze, W., and Horst, P., "Preliminary Design of a Blended Wing Body Configuration Using the Design Tool PrADO," *Proceedings of the CEAS Conference on Multidisciplinary Aircraft Design and Optimisation*, Confederation of European Aerospace Societies, Cologne, Germany, 2001, pp. 1–10.

[14] Werner-Westphal, C., Heinze, W., and Horst, P., "Multidisciplinary Integrated Preliminary Design Applied to Future Green Aircraft Configurations," *Proceedings of the 45th AIAA Aerospace Sciences Meeting and Exhibit*, AIAA, Reston, VA, 2007, pp. 1–13.

[15] Rieke, J., Heinze, W., Horst, P., and Schwochow, J., "Evaluation of Flutter Analysis in the Context of New Concepts of Preliminary Aircraft Design," *Jahrbuch des Deutschen Luft- und Raumfahrtkongresses*, Deutsche Gesellschaft für Luft- und Raumfahrttechnik, Braunschweig, Germany, 2006, pp. 743–751.

[16] "Abschätzung der Rißfortschrittsraten für Metallische Werkstoffe mit Hilfe der Forman-Gleichung," *Handbuch Struktur Berechnung*, Industrie Ausschuss Struktur Berechnungsunterlagen, Ottobrun, 1989, p. 63205-01.

[17] Krueger, R., "Virtual Crack Closure Technique: History, Approach, and Applications," *Applied Mechanics Reviews*, Vol. 57, No. 2, 2004, pp. 109–143. doi:10.1115/1.1595677

[18] Ewalds, H. L., and Wanhill, R. J. H., *Fracture Mechanics*, Edward Arnold, London, 1989.

[19] Gieger, M., and Ermanni, P., "Development of CFRP Racing Motorcycle Rims Using a Heuristic Evolutionary Approach," *Structural and Multidisciplinary Optimization*, Vol. 30, No. 2, 2005, pp. 54–65. doi:10.1007/s00158-004-0471-3

[20] König, O., "Evolutionary Design Optimization: Tools and Applications," Ph.D.-Dissertation, Swiss Federal Inst. of Technology, Zurich, 2004.

[21] Marler, R. T., and Arora, J. S., "Survey of Multi-Objective Optimization Methods for Engineering," *Structural and Multidisciplinary Optimization*, Vol. 26, No. 6, 2004, pp. 369–395. doi:10.1007/s00158-003-0368-6